2007

Sensitivity of Pan-Arctic Terrestrial Net Primary Productivity Simulations to Daily Surface Meterology From NCEP-NCAR and ERA-40 Reanalyses

Ke Zhang

John S. Kimball

Maosheng Zhao

Walter C. Oechel

John Cassano

See next page for additional authors

JOURNAL OF GEOPHYSICAL RESEARCH, VOL. 112, G01011, doi:10.1029/2006JG000249, 2007

Sensitivity of pan-Arctic terrestrial net primary productivity simulations to daily surface meteorology from NCEP-NCAR and ERA-40 reanalyses

Ke Zhang,[1,2] John S. Kimball,[1,2] Maosheng Zhao,[2] Walter C. Oechel,[3] John Cassano,[4] and Steven W. Running[2]

Received 19 June 2006; revised 12 October 2006; accepted 23 October 2006; published 7 February 2007.

[1] We applied a terrestrial net primary production (NPP) model driven by satellite remote sensing observations of vegetation properties and daily surface meteorology from the 45-year ECMWF Re-Analysis (ERA-40) and the National Centers for Environmental Prediction/National Center for Atmospheric Research (NCEP-NCAR) reanalysis (NNR) to assess NPP spatial and temporal variability for the pan-Arctic basin and Alaska from 1982 to 2000. Sensitivity analysis of the production efficiency model (PEM) to uncertainties in surface meteorological inputs indicate that ERA-40 solar radiation and NNR solar radiation and surface temperatures are the primary sources of PEM-based NPP uncertainty for the region. Considerable positive bias in solar radiation inputs relative to surface observation networks resulted in overprediction of annual NPP by approximately 35.2 and 61.6% using ERA-40 and NNR inputs, respectively. Despite these uncertainties, both reanalysis products captured the major annual anomalies and trends in surface meteorology for the domain. The two reanalysis products also produced similar NPP spatial patterns for 74.7% of the domain, and similar annual anomalies and temporal trends, though there were significant regional differences particularly for Eurasia. A simple correction method based on a sensitivity experiment between reanalysis and surface station meteorological measurements produced generally consistent NPP results that were considerably smaller than PEM simulations derived from uncorrected reanalysis drivers. The results of this study identify major sources of uncertainty in reanalysis-based surface meteorology, and associated impacts on regional NPP simulations of the northern high latitudes.

Citation: Zhang, K., J. S. Kimball, M. Zhao, W. C. Oechel, J. Cassano, and S. W. Running (2007), Sensitivity of pan-Arctic terrestrial net primary productivity simulations to daily surface meteorology from NCEP-NCAR and ERA-40 reanalyses, *J. Geophys. Res.*, *112*, G01011, doi:10.1029/2006JG000249.

1. Introduction

[2] Boreal forest and Arctic tundra biomes of the pan-Arctic basin and Alaska encompass approximately 25 million km^2 of the northern high (>50°N) latitudes and 30% of the combined North American and Eurasian landmass [*Kimball et al.*, 2006]. The biomes in this region contain up to 40% of the global terrestrial carbon reservoir [*Saugier et al.*, 2001; *Lal and Kimble*, 2000]. This region is currently undergoing significant change coinciding with recent and persistent climatic warming [*Serreze et al.*, 2000; *Comiso*, 2003]. Ecosystem responses to these changes include thawing permafrost and increases in soil active layer depths, advances in the timing and length of seasonal growing seasons, increased vegetation structure and growth, and alteration of land-atmosphere CO_2 exchange [*Oelke et al.*, 2004; *Sturm et al.*, 2001; *McDonald et al.*, 2004; *Oechel et al.*, 2000; *Lucht et al.*, 2002].

[3] Terrestrial Net Primary Production (NPP) is the net carbon fixed by vegetation from the atmosphere and equals the difference between photosynthesis or gross primary production (GPP) and autotrophic respiration. Boreal and Arctic NPP is characteristically low compared to temperate forests owing to reduced solar radiation, cold temperatures and shorter growing seasons relative to lower latitudes. Cold temperatures, permafrost and wet soils also inhibit soil decomposition and heterotrophic respiration processes, resulting in a general historical pattern of net annual uptake of atmospheric CO_2 and subsequent large accumulations of soil organic carbon. Recent warming trends may be enhanc-

[1]Flathead Lake Biological Station, Division of Biological Sciences, University of Montana, Polson, Montana, USA.
[2]Numerical Terradynamic Simulation Group, Department of Ecosystem and Conservation Sciences, University of Montana, Missoula, Montana, USA.
[3]Global Change Research Group, Biology Department, San Diego State University, San Diego, California, USA.
[4]Cooperative Institute for Research in Environmental Sciences and Department of Atmospheric and Oceanic Sciences, University of Colorado, Boulder, Colorado, USA.

0148-0227/07/2006JG000249$09.00

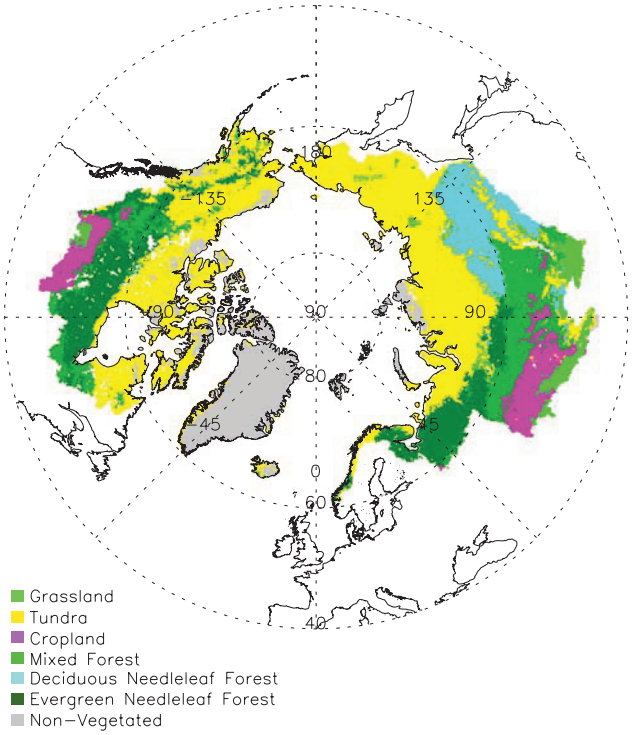

Figure 1. Land cover classification of the pan-Arctic basin and Alaska domain derived from a NOAA AVHRR based global land cover classification.

ing carbon sequestration by increasing vegetation growth. However, warming may also be enhancing carbon losses by increasing vegetation stress, soil decomposition, carbon volatilization and respiration processes [*Oechel et al.*, 1995, 2000; *Stocks et al.*, 2002; *Barber et al.*, 2000].

[4] Several recent studies have been conducted to assess regional- to global-scale patterns and trends in vegetation productivity using biogeochemical or production efficiency models driven by satellite remote sensing observations and surface station or reanalysis meteorological data [*Kimball et al.*, 2006; *Zhao et al.*, 2006; *Nemani et al.*, 2003; *Goetz et al.*, 2005; *Bunn et al.*, 2005; *Lucht et al.*, 2002]. Though some discrepancies exist in the various estimates of plant productivity change, the general consensus of these studies is that plant growth displayed a predominantly positive trend for the northern terrestrial high latitudes during the 1980s and 1990s. Much of the uncertainty in these regional trends, however, may be due to the relative accuracy of the driving data used to predict vegetation photosynthetic activity and NPP. Surface meteorological station networks are extremely sparse across the high northern latitudes, while reanalysis meteorological data sets are based on assimilation of sparse surface and upper air data and satellite data using coarse resolution atmospheric models. Satellite remote sensing at optical-IR wavelengths is also problematic at high northern latitudes owing to reduced solar illumination, frequent cloud cover and atmospheric aerosol contamination effects [*Zhao et al.*, 2005], while long-term monitoring from these data are influenced by instrumental and navigational drift, and intercalibration of successive instruments [*Cihlar et al.*, 1997].

[5] The objective of this investigation was to assess the sensitivity and relative uncertainty of regional NPP simulations of the pan-Arctic basin and Alaska in response to uncertainties in surface meteorological inputs. We conducted regional simulations of NPP spatial patterns and temporal trends for the region from 1982 to 2000 using a biome-specific production efficiency model (PEM) driven by daily surface meteorology and satellite remote sensing observations of photosynthetic leaf area. Owing to the extremely sparse surface weather station network at high latitudes, we chose two spatially contiguous reanalysis meteorological data sets as the primary input meteorological drivers for this investigation; namely, surface air temperature, humidity and incident solar radiation from the 45-year ECMWF Re-Analysis (ERA-40) and the NCEP-NCAR reanalysis (NNR). We evaluated the relative accuracy of reanalysis daily surface meteorology using available surface station network measurements, and the response of PEM based NPP spatial patterns, annual anomalies and regional trends to differences in reanalysis meteorological drivers.

2. Data Sets and Methodology

2.1. Study Area

[6] The study domain encompasses the pan-Arctic basin and Alaska including all land areas draining into the Arctic Ocean, Hudson Bay, James Bay, Hudson Strait and the Bering Sea (Figure 1). The region is defined in terms of nodes of the National Snow and Ice Data Center (NSIDC) north polar Equal-Area Scalable Earth (EASE) grid [*Armstrong and Brodzik*, 1995]. The study domain spans a latitudinal range from 45.35°N to 83.62°N, while land areas within the region comprise 39,926 grid cells with nominal 25 km × 25 km resolution and a total representative area of approximately 25 million km^2. A NOAA AVHRR based global land cover classification was also used to define major biomes within the study region [*Myneni et al.*, 1997; *DeFries et al.*, 1998].

2.2. Production Efficiency Model Calculations

[7] A biome-specific Production Efficiency Model (PEM), i.e., MODIS MOD17A2/A3 algorithms, was used to calculate GPP and NPP for vegetated grid cells within the 25-km resolution EASE-grid domain using monthly estimates of satellite-derived vegetation properties and daily surface meteorological data. The PEM model is based on the original logic of *Monteith* [1972] and combined with climatic controls on NPP [*Churkina and Running*, 1998] and lessons learned from a general process-based ecosystem model, BIOME-BGC [*Running and Hunt*, 1993; *Thornton and Running*, 1999; *White et al.*, 2000]. The model is driven by satellite-derived land cover, fractional photosynthetically active radiation (FPAR), leaf area index (LAI) as well as surface daily meteorology [*Running et al.*, 2000]. The model has been successfully applied at global or regional scales [e.g., *Nemani et al.*, 2003; *Zhao et al.*, 2005, 2006; *Kimball et al.*, 2006] and has undergone several revisions in response to extensive, ongoing calibration and verification studies using biophysical information from regional station networks, including boreal and Arctic landscapes [e.g., *Heinsch et al.*, 2006; *Turner et al.*, 2003, 2005; *Zhao et al.*, 2005, 2006]. In this study, we used satellite-derived

vegetation properties including monthly FPAR and LAI from the NOAA AVHRR Pathfinder (PAL) 16 km data set [*Myneni et al.*, 1997]. The LAI and FPAR data are based on a monthly maximum value compositing of AVHRR spectral reflectance data to mitigate cloud cover, smoke, and other atmospheric aerosol contamination effects. These data were reprojected to the 25-km polar EASE-grid format using a nearest-neighbor resampling scheme. The monthly LAI and FPAR data were then resampled to a daily time step by temporal linear interpolation of adjacent monthly values. The daily linear interpolation approach used for this investigation is a relatively simple, but effective means for producing a daily FPAR and LAI time series for PEM simulations and has been used extensively for global vegetation analyses of the AVHRR Pathfinder series [*Myneni et al.*, 1997; *Nemani et al.*, 2003]. GPP (g C m^{-2}) was derived on a daily basis as [*Running et al.*, 2000, 2004; *Heinsch et al.*, 2003; *Nemani et al.*, 2003],

$$GPP = \varepsilon \cdot FPAR \cdot PAR \tag{1}$$

$$\varepsilon = \varepsilon_{\max} \cdot T_f \cdot VPD_f, \tag{2}$$

where ε is a light use efficiency parameter (g C MJ^{-1}) for the conversion of photosynthetically active radiation (PAR, MJ m^{-2}) to GPP, where PAR is assumed to represent 45% of incident solar radiation; $\varepsilon_{\max}$ is the potential maximum ε under optimal conditions; T_f is a scalar that defines reductions in photosynthesis under low temperature conditions, while VPD_f is a scalar that defines similar reductions under suboptimal surface air Vapor Pressure Deficit (*VPD*) and associated daytime water stress conditions. Both T_f and VPD_f are defined from daily minimum air temperature ($T_{\min}$) and mean daily *VPD* using simple photosynthetic response curves.

[8] Net primary production (NPP, g C m^{-2}) is derived on an annual basis as the difference between the annual summation of daily net photosynthesis and autotrophic growth and maintenance respiration,

$$NPP = \sum_{1}^{365} (GPP - R_{m\_lr}) - \left(R_{m\_w} + R_g\right), \tag{3}$$

where R_{m_lr} is the daily maintenance respiration of leaves and fine roots; R_{m_w} represents the annual maintenance respiration from live wood; and R_g represents annual growth respiration. The characteristic response curves for calculating these parameters vary according to major biomes as defined by a Biome Properties Look-Up Table (BPLUT), which was developed from stand level ecophysiological studies [*White et al.*, 2000] and adjusted for the effects of regional meteorological and satellite-based FPAR/LAI data sets [*Running et al.*, 2000; *Zhao et al.*, 2005]. To drive the model, satellite-derived land cover, and FPAR and LAI data were used with observed and reanalysis daily surface meteorological data including incident solar radiation (SW_{rad}), minimum and average air temperatures ($T_{\min}$, T_{avg}), and *VPD* to derive daily GPP and NPP across the domain. In this study, *VPD* is calculated from daily average air temperature (T_{avg}) and mean daily atmospheric vapor pressure (e_a). Therefore the actual PEM daily climate drivers include SW_{rad}, $T_{\min}$, T_{avg} and e_a.

2.3. Meteorological Data Sets

[9] In this study, we chose two meteorological data sets: the National Centers for Environmental Prediction-National Center for Atmospheric Research (NCEP-NCAR) reanalysis (NNR) [*Kistler et al.*, 2001; *Kalnay et al.*, 1996] and the 45-year European Centre for Medium-Range Weather Forecasts (ECMWF) Re-Analysis (ERA-40) [*Uppala et al.*, 2005]. Because the AVHRR PAL LAI/FPAR data are only available from July 1981 to May 2001, we chose 1982–2000 as our study period. This time period is also consistent with several recent model and satellite remote sensing based assessments of high-latitude NPP changes [*Lucht et al.*, 2002; *Nemani et al.*, 2003; *Kimball et al.*, 2006].

[10] NNR is a first-generation reanalysis from 1948, which uses a frozen state-of-the-art analysis/forecast system and performs data assimilation using a variety of surface measurements to guide model simulations, including land surface, ship, rawinsonde, pibal, aircraft, satellite and other data [*Kalnay et al.*, 1996]. There are several documented problems with the NNR (http://www.cdc.noaa.gov/cdc/reanalysis/problems.shml), including model characterization of fractional cloud cover and an error in the surface skin temperature calculation, which may also affect air temperature calculations. In this study, we chose NCEP/NCAR Reanalysis 1: Surface Flux product (http://www.cdc.noaa.gov/cdc/data.ncep.reanalysis.surfaceflux.html), which is provided four times per day in a global Gaussian grid (T62, 192 × 94 points) format with approximately 1.9° × 1.875° spatial resolution. The extracted data include surface downward solar radiation, surface air pressure, 2-m specific humidity, average air temperature and extreme temperatures. The e_a term used to derive daily *VPD* was calculated from NNR specific humidity and surface pressure information. The ERA-40 product is a 45-year, second-generation reanalysis carried out by ECMWF that benefits from many recent changes made to the operational ECMWF data assimilation system, and lessons learned from the earlier ERA-15 reanalysis [*Uppala et al.*, 2005]. The observations used for ERA-40 include data from the operational archives of ECMWF supplemented by operational data archived by NCEP and the Japan Meteorological Agency. We used the ERA-40 Basic Atmospheric Data Sets product (http://www.ecmwf.int/products/data/archive/descriptions/e4/basic.html), which is produced with four times per day temporal repeat at 2.5° × 2.5° spatial resolution and is similar to the NNR resolution, though other ERA-40 data products are available at finer spatial resolutions. Surface downward solar radiation and 2-m air and dew point temperatures from the ERA-40 reanalysis were extracted for this investigation. Atmospheric vapor pressure (e_a) was calculated from the daily dew point, while *VPD* was derived as the daily difference between e_a and the saturation vapor pressure of the mean daytime air temperature.

[11] The NNR is based on the NCEP global spectral model with 28 vertical "sigma" levels and a triangular truncation of 62 waves (T62), whereas ERA-40 uses an improved data assimilation system and a T159 model with 60 hybrid sigma-pressure levels, and more observational data than previous reanalyses [*Santer et al.*, 2004; *Uppala et*

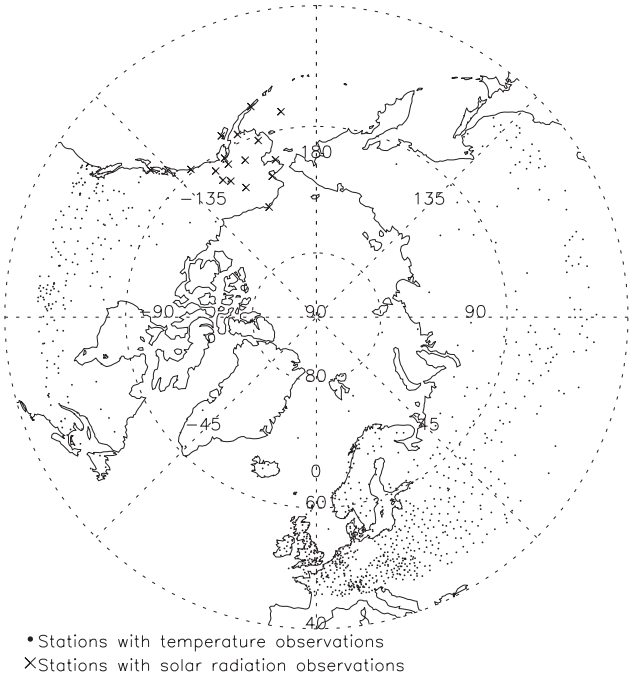

Figure 2. Distribution of surface weather stations with daily temperature and dew point observations, and solar radiation observations.

al., 2005; *Wang et al.*, 2006]. Some studies have shown a clear improvement of ERA-40 over the earlier NNR during the modern satellite era (post 1978) [*Uppala et al.*, 2005; *Bromwich and Fogt*, 2004]. *Bromwich and Fogt* [2004] found that ERA-40 produced a generally improved simulation of mean sea level pressure fields after 1978 based on comparisons with Antarctic and southern hemisphere mid- to high-latitude station observations. *Simmons et al.* [2004] found that ERA-40 produced generally closer agreement for simulated surface air temperatures from 1979 onward on the basis of comparisons with the Climatic Research Unit (CRU) CRUTEM2v data set, which is derived directly from monthly surface weather station observations. *Bromwich and Wang* [2005] also found that ERA-40 showed better overall performance in representing wind fields of the Arctic on the basis of comparisons with the rawinsonde data for two independent arctic field experiments.

[12] We used daily minimum and average air temperatures and dew point temperatures from 1994–2000 for 1122 World Meteorology Organization (WMO) stations (Figure 2) to assess the relative accuracy of the reanalysis meteorological inputs across the pan-Arctic domain. These data were obtained from the National Climatic Data Center Climate Services Branch (NCDC CSB; http://www.ncdc.noaa.gov) Global Surface Summary of the Day. We also evaluated reanalysis daily solar radiation inputs using daily solar radiation data from 17 sites distributed across Alaska from 1982–1990, and available from the National Solar Radiation Data Base (NSRDB; http://rredc.nrel.gov/solar/old_data/nsrdb/). To compare the reanalysis data with the station observations, we applied *Zhao et al.*'s [2005, equation 3–5] spatial interpolation method to calculate the reanalysis values at the sites of the weather stations. Analyses of statistical bias, linear least squares correlation and root mean square error (RMSE) parameters were then used to evaluate accuracy and uncertainty of the two reanalyses by comparing the interpolated values with surface weather station observations.

2.4. Uncertainty and Sensitivity Analysis of PEM Output

[13] We constructed the following experimental model to determine the effects of NNR/ERA-40 reanalysis meteorological uncertainty on PEM based NPP calculations,

$$Y = f\left(\tilde{d}_{SW_{\mathrm{rad}}}, \nabla\tilde{T}_{\mathrm{avg}}, \nabla\tilde{T}_{\mathrm{min}}, \nabla\tilde{e}_{\mathrm{a}}\right), \tag{4}$$

where $\tilde{d}_{SW_{\mathrm{rad}}}$, $\nabla\tilde{T}_{\mathrm{avg}}$, $\nabla\tilde{T}_{\mathrm{min}}$ and $\nabla\tilde{e}_{\mathrm{a}}$ are the samples from $d_{SW_{\mathrm{rad}}}$, ∇T_{avg}, ∇T_{min} and ∇e_{a} populations, respectively, which are defined as follows:

$$d_{SW_{\mathrm{rad}}} = \frac{SW_{\mathrm{rad,Obs}}}{SW_{\mathrm{rad,Res}}}, \tag{5}$$

$$\nabla T_{\mathrm{avg}} = T_{\mathrm{avg,Obs}} - T_{\mathrm{avg,Res}}, \tag{6}$$

$$\nabla T_{\mathrm{min}} = T_{\mathrm{min,Obs}} - T_{\mathrm{min,Res}}, \tag{7}$$

$$\nabla e_{\mathrm{a}} = e_{\mathrm{a,Obs}} - e_{\mathrm{a,Res}}, \tag{8}$$

where *Obs* denotes the observed value and *Res* denotes the reanalysis value. We multiplied $SW_{\mathrm{rad,Res}}$ by $\tilde{d}_{SW_{\mathrm{rad}}}$, added $\nabla\tilde{T}_{\mathrm{avg}}$ to $T_{\mathrm{avg,Res}}$, added $\nabla\tilde{T}_{\mathrm{min}}$ to $T_{\mathrm{min,Res}}$ and added $\nabla\tilde{e}_{\mathrm{a}}$ to $e_{\mathrm{a,Res}}$ to produce the experimental input data. We used both reanalysis and experimental data with the PEM model to calculate NPP. Finally, we determined Y by subtracting the NPP driven by the original reanalysis data from the corresponding experimental input data-based NPP results. This provided a relatively simple approach for quantifying PEM error due to input data uncertainty, since Y denotes NPP variability resulting from differences between surface observation and reanalysis meteorological inputs.

[14] To quantify the uncertainty of reanalysis surface meteorology, we first constructed cumulative distribution functions (CDFs) of $d_{SW_{\mathrm{rad}}}$, ∇T_{avg}, ∇T_{min} and ∇e_{a}. Then, we used a Latin hypercube approach [*Helton and Davis*, 2003] to sample input variables of the experimental model by: (1) dividing the range of each variable into nS (nS = 99 in this experiment) disjoint intervals of equal probability and selecting one value randomly from each interval; (2) pairing the nS values of $\tilde{d}_{SW_{\mathrm{rad}}}$ randomly without replacement with the nS values for $\nabla\tilde{T}_{\mathrm{avg}}$ to produce nS pairs; (3) combining the nS pairs randomly without replacement with the nS values for $\nabla\tilde{T}_{\mathrm{min}}$ to produce nS triples; and (4) combining the nS triples randomly without replacement with the nS values for $\nabla\tilde{e}_{\mathrm{a}}$ to produce nS quadruples. We used the nS samples to drive the experimental model for the six general biome types defined by the regional land cover map and derived corresponding scatterplots of Y against $d_{SW_{\mathrm{rad}}}$, ∇T_{avg}, ∇T_{min} and ∇e_{a} for both reanalyses.

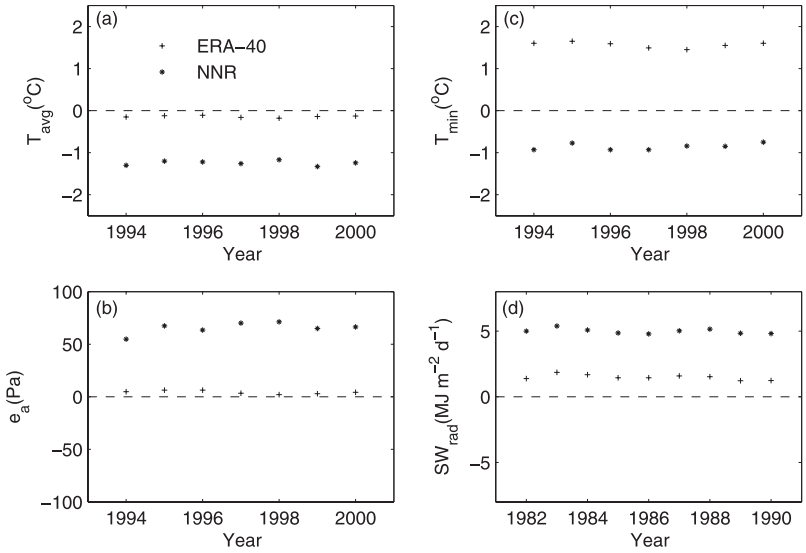

Figure 3. Temporal comparison of mean annual bias (reanalysis - observations) in NNR and ERA-40 surface (a) daily average air temperature, (b) daily mean atmospheric vapor pressure, (c) daily minimum air temperature, and (d) daily downward solar radiation relative to observations from WMO and NSRDB station data.

[15] To determine whether the distribution of points in the scatterplots is nonrandom, (i.e., the significance of $d_{SW_{rad}}$, ∇T_{avg}, ∇T_{min} and ∇e_a effects on Y), we used (1) statistical independence (SI) and (2) entropy tests [*Helton et al.*, 2006]. Both of these tests are based on a gridding method. In this study, we used a 5 by 5 grid. We (1) divided the range of x ($d_{SW_{rad}}$, ∇T_{avg}, ∇T_{min} and ∇e_a) into n_x ($n_x = 5$) mutually exclusive and exhaustive subintervals containing equal numbers of sampled values, (2) divided the range of y (i.e., Y) into n_y ($n_y = 5$) mutually exclusive and exhaustive subintervals containing equal numbers of sampled values, and (3) counted the number of each cell nO_{rc}. The statistic in the SI test is defined as

$$T = \sum_{c=1}^{n_x} \sum_{r=1}^{n_y} (nO_{rc} - nE_{rc})^2 / nE_{rc}, \tag{9}$$

where $nE_{rc} = nS/(n_x \cdot n_y)$is an estimate of the expected number of observations that should fall in cell (r,c); and $nS = 99$ is the sample size. Asymptotically, T follows a χ^2-distribution with $(n_x - 1)$ $(n_y - 1)$ degrees of freedom when x and y are independent. Thus $prob_{\chi^2}\lfloor \tilde{T} > T | (n_x - 1)(n_y - 1) \rfloor$is the probability (i.e., p-value) of obtaining a value of $\tilde{T}$ that exceeds T when x and y are independent. Measures of entropy provide another grid-based procedure to assess the strength of nonlinear relationships between x and y. The following quantities are defined as [*Helton et al.*, 2006]:

$$H(y) = -\sum_{r=1}^{n_y} (n_{y_r}/nS) \ln(n_{y_r}/nS), \tag{10}$$

$$H(x) = -\sum_{c=1}^{n_x} (n_{x_c}/nS) \ln(n_{x_c}/nS), \tag{11}$$

$$H(y,x) = -\sum_{r=1}^{n_y} \sum_{c=1}^{n_x} (nO_{rc}/nS) \ln(nO_{rc}/nS), \tag{12}$$

$$U(y,x) = 2[H(y) + H(x) - H(y,x)]/[H(y) + H(x)], \tag{13}$$

where n_{x_c} is the number of points following in column c; n_{y_r} is the number of points following in row r; $H(y)$ and $H(x)$ are estimates of the entropy associated with y and x; and $U(y,x)$ is the entropy-based measure of the strength of the association between x and y.

3. Results and Discussion

3.1. Comparison of Meteorological Data Sets

[16] The four meteorological variables show no obvious temporal bias (relative to surface weather station observations), i.e., temporally independent for both reanalyses (Figure 3). Both reanalyses underestimate T_{avg}, while ERA-40 has a smaller bias and RMSE and higher correlation with surface observations than NNR (Table 1). For T_{min}, ERA-40 has a positive bias whereas NNR has a negative bias and smaller absolute bias. However, ERA-40 T_{min} has a smaller RMSE and a higher correlation with the observations than NNR T_{min} does. For e_a, ERA-40 has a much smaller bias and RMSE, and a higher correlation with the observations than NNR, though both reanalyses have positive biases. While instrumentation biases and inhomogeneities may exist in the weather station observational data, we chose a large station sample size (1122 stations) to minimize the potential negative effects of individual station bias and compared these data with the interpolated reanalyses data. The results of these comparisons indicate that ERA-40 is generally more accurate than NNR for surface air temperature and atmospheric vapor pressure, though both reanalyses show similar long-term temperature

Table 1. Comparison of Bias, RMSE, and Simple Correlation Coefficient (r) of Reanalysis Mean Daily Meteorological Data Relative to Surface Weather Station Observations

	ERA-40 Reanalysis				NNR			
	Bias	RMSE	r	P[a]	Bias	RMSE	r	P[a]
Mean Values								
T_{avg},[b] °C	−0.14	1.593	0.944	<0.0001	−1.24	2.417	0.912	<0.0001
T_{min},[b] °C	1.56	2.295	0.947	<0.0001	−0.86	2.556	0.903	<0.0001
e_a,[b] Pa	4.32	75.08	0.928	<0.0001	65.52	110.15	0.898	<0.0001
SW_{rad},[c] MJ m^{-2} d^{-1}	1.407	1.852	−0.569	0.0099	4.92	5.13	0.518	0.0180
Anomalies								
T_{avg},[d] °C	Z[f]	0.025	0.999	<0.0001	Z[f]	0.056	0.993	<0.0001
T_{min},[d] °C	Z[f]	0.070	0.989	<0.0001	Z[f]	0.077	0.993	<0.0001
e_a,[d] Pa	Z[f]	1.656	0.998	<0.0001	Z[f]	5.444	0.975	0.0084
SW_{rad},[e] MJ m^{-2} d^{-1}	Z[f]	0.259	0.243	0.2234	Z[f]	0.239	0.043	0.4471

[a]P denotes the P-value.
[b]The surface meteorological data are 7-year daily means over the 1994 to 2000 period; the observations come from 1122 weather stations across the domain.
[c]The solar radiation data are 9-year daily means over the 1982 to 1990 period; the observations come from 17 weather stations in Alaska.
[d]The anomalies include 7-year values.
[e]The anomalies include 9-year values.
[f]Bias of anomaly is equal to zero.

trends. These results are also consistent with the previous studies [*Simmons et al.*, 2004; *Zhao et al.*, 2006]. Both reanalyses also show relatively poor performance for solar radiation, though ERA-40 has a lower bias than NNR. While both reanalyses consider cloud effects, generally poor reanalysis performance relative to surface observations likely reflects limitations in the way the atmospheric models characterize cloud cover heterogeneity and atmospheric solar radiation transmittance. In ERA-40, cloud radiative properties relate more to model parameterization than to the quality of the basic reanalysis fields and are not well simulated, leading to relatively poor characterization of the all-sky radiation budget [*Uppala et al.*, 2005]. The study of *Yang et al.* [1999] suggested that the NNR global data assimilation system (GDAS) contains shortcomings in the cloud/moisture parameterizations or deficiencies in the shortwave parameterizations, which lead to the large bias in solar radiation. In addition, while these results indicate generally poor model performance for solar radiation, they are based on comparisons with surface observations from only 17 stations across Alaska. Model solar radiation performance is likely to vary across the larger pan-Arctic domain and may not be adequately defined from this limited observation network.

[17] Analysis of ERA-40 performance (Table 2) shows no obvious longitudinal pattern in temperature and e_a accuracies. However, ERA-40 temperatures and e_a show generally better performance in the Arctic relative to Boreal biomes. The NNR performance also showed no obvious longitudinal pattern, but showed a latitudinal pattern in e_a accuracies. The relatively high temporal, spatial and anomaly correlation coefficients between the reanalyses and surface observations also indicate that both NNR and ERA-40 products capture the major climatic patterns and trends for surface air temperature.

[18] Analysis of the 1982–2000 meteorological trends for the domain showed a small, insignificant ($P > 0.1$) decrease in incident solar radiation of −5.41 MJ m^{-2} per decade and

Table 2. Regional Comparison of Annual Means of Daily Air Temperatures (T_{min} and T_{avg}) and Daily Mean Atmospheric Vapor Pressure (e_a) From the Two Reanalyses Relative to Observed Values Across the Pan-Arctic Domain[a]

			T_{min}, °C			T_{avg}, °C			e_a, Pa		
Classification Region	Area,[b] %		r[c]	Bias	RMSE	r	Bias	RMSE	r	Bias	RMSE
Pan-Arctic	100.0	E[d]	0.95	1.56	2.32	0.94	−0.14	1.61	0.93	4.32	77.78
		N[e]	0.90	−0.85	2.60	0.91	−1.24	2.45	0.89	65.52	113.73
North America	33.7	E	0.93	1.29	2.36	0.95	−0.73	1.78	0.90	−26.10	81.39
		N	0.88	−1.37	2.92	0.92	−2.28	3.13	0.86	56.76	110.09
Eurasia	66.3	E	0.94	1.65	2.37	0.93	0.04	1.66	0.91	11.74	81.21
		N	0.88	−1.04	2.60	0.89	−1.12	2.37	0.86	65.36	118.32
Boreal	39.0	E	0.93	1.62	2.34	0.91	0.10	1.63	0.90	4.50	81.82
		N	0.87	−0.77	2.55	0.86	−1.17	2.42	0.85	68.26	118.55
Arctic	33.2	E	0.96	1.23	2.22	0.97	−0.35	1.49	0.95	3.32	47.86
		N	0.92	−1.35	2.91	0.94	−1.66	2.58	0.92	49.49	80.01

[a]The results are summarized for major sub-regions within the domain.
[b]Proportional area represented within the entire 25 million km^2 study domain.
[c]Here r denotes the simple correlation coefficient between surface observations and reanalysis data.
[d]E denotes ERA-40.
[e]N denotes NNR.

Table 3. Comparison of Grid-Based SI Test and Entropy Values Between Sensitivity Experiment and ERA-40 and NNR Uncertainty

	ERA-40				NNR			
		SI Test[a]				SI Test		
	Variable	χ^2 [b]	*P*-Value	Entropy $U(y,x)$[a]	Variable	χ^2	*P*-Value	Entropy $U(y,x)$
Evergreen needleleaf forest	$d_{SW_{rad}}$	109.33	<0.0001	0.3814	$d_{SW_{rad}}$	50.24	<0.0001	0.1580
	∇T_{avg}	33.07	0.0072	0.1352	∇T_{avg}	46.71	0.0001	0.1497
	∇T_{min}	27.52	0.0361	0.0868	∇T_{min}	31.56	0.0114	0.1174
	∇e_a	15.90	0.4600	0.0514	∇e_a	10.85	0.8186	0.0328
Deciduous needleleaf forest	$d_{SW_{rad}}$	108.83	<0.0001	0.3446	$d_{SW_{rad}}$	57.31	<0.0001	0.1665
	∇T_{avg}	41.66	0.0004	0.1608	∇T_{avg}	41.15	0.0005	0.1367
	∇T_{min}	30.04	0.0178	0.1005	∇T_{min}	34.08	0.0053	0.1172
	∇e_a	14.89	0.5327	0.0482	∇e_a	12.36	0.7188	0.0359
Mixed forest	$d_{SW_{rad}}$	120.44	<0.0001	0.3900	∇T_{avg}	53.78	<0.0001	0.1834
	∇T_{avg}	36.61	0.0024	0.1448	$d_{SW_{rad}}$	38.63	0.0012	0.1247
	∇T_{min}	32.57	0.0084	0.1198	∇T_{min}	29.03	0.0237	0.1013
	∇e_a	13.37	0.6455	0.0450	∇e_a	8.32	0.9388	0.0252
Tundra	$d_{SW_{rad}}$	104.28	<0.0001	0.3599	$d_{SW_{rad}}$	53.78	<0.0001	0.1866
	∇T_{min}	38.63	0.0012	0.1197	∇T_{min}	52.26	<0.0001	0.1576
	∇T_{avg}	21.96	0.1445	0.0825	∇T_{avg}	30.55	0.0154	0.1014
	∇e_a	15.90	0.4600	0.0505	∇e_a	11.35	0.7874	0.0389
Grassland	$d_{SW_{rad}}$	110.34	<0.0001	0.3785	∇T_{min}	46.71	0.0001	0.1588
	∇T_{min}	37.62	0.0017	0.1137	$d_{SW_{rad}}$	44.69	0.0002	0.1362
	∇T_{avg}	26.00	0.0540	0.0953	∇T_{avg}	33.58	0.0062	0.1120
	∇e_a	20.44	0.2011	0.0641	∇e_a	9.84	0.8748	0.0314
Cropland	$d_{SW_{rad}}$	124.99	<0.0001	0.4087	$d_{SW_{rad}}$	52.77	<0.0001	0.1684
	∇T_{avg}	33.07	0.0072	0.1352	∇T_{avg}	40.14	0.0007	0.1343
	∇T_{min}	31.05	0.0133	0.1019	∇T_{min}	23.98	0.0899	0.0771
	∇e_a	13.37	0.6455	0.0641	∇e_a	11.86	0.7536	0.0346

[a]Both SI test and entropy test were based on a 5 × 5 grid.
[b]The degrees of freedom were 16.

-11.98 MJ m^{-2} d^{-1} per decade for ERA-40 and NNR, respectively. Mean surface daily air temperatures showed a small increase of 0.48°C per decade (P = 0.006) and 0.24°C per decade (P = 0.08) for ERA-40 and NNR, respectively. There was no discernable regional trend in surface minimum daily air temperature from either reanalysis product. Mean daily e_a for the region showed a small increase of 15.56 Pa per decade (P = 0.003) and 5.03 Pa per decade (P = 0.18) for ERA-40 and NNR, respectively. Overall the two reanalyses showed generally consistent pan-Arctic regional trends for the four meteorological variables. These results are also in general agreement with other reported regional observations. The *Intergovernmental Panel on Climate Change* [2001] reported a significant warming trend in the Arctic for the period 1976 to 2000. *Wang and Key* [2003] reported that the land surface temperature of the Arctic has increased at a rate of 0.54°C per decade over the 1982 to 1999 period on the basis of satellite observations. They also reported an Arctic annual trend in net cloud forcing of surface solar radiation of approximately -3.17 W m^{-2} due to increasing cloud cover over land.

3.2. Results of Uncertainty and Sensitivity Analysis

[19] The results of the SI and entropy tests are presented in Table 3. The higher values for χ^2 and $U(y, x)$ indicate that y is more sensitive to x. We also calculated the P-value for the χ^2 test (Table 3). These results are similar for both SI and entropy tests and indicate that PEM based NPP derived from ERA-40 is primarily sensitive to uncertainty in SW_{rad}, followed by air temperatures (T_{min} and T_{avg}) as a significant source of model uncertainty for all major biomes within the domain. However, the relative importance of T_{min} and T_{avg} to PEM based NPP varies for individual biome types. Though ERA-40 shows generally more accurate representation of T_{min} than T_{avg} (Figure 3 and Table 1), the uncertainty in T_{avg} yields similar impacts on PEM based NPP as the uncertainty in T_{min}. This response occurs because T_{avg} controls model calculations of *VPD* and vegetation autotrophic respiration. When T_{avg} is underestimated (Figure 3), both respiration and *VPD* are correspondingly underestimated. The latter result can also lead to the overestimation of GPP. The coupled effects of these processes can therefore magnify model sensitivity to T_{avg} error. ERA-40 shows relatively accurate representation of e_a; relative to the above parameters, e_a uncertainty for this investigation did not have a significant impact on PEM based NPP results.

[20] Analyses of the PEM results derived from the NNR daily meteorology are similar to the ERA-40 based results and indicate that SW_{rad} and temperatures (T_{min} and T_{avg}) are the most important sources of model NPP uncertainty. Uncertainty in NNR e_a also had the lowest impact on PEM based NPP. The generally low accuracy of SW_{rad} and considerable biases in temperature inputs (Figure 1 and Tables 1 and 2) relative to e_a uncertainty yield much larger negative impacts on PEM based NPP results.

[21] Overall, these results show considerable uncertainties in both reanalyses, that significantly impact the spatial and temporal accuracy of PEM based NPP calculations. The ability of regional models to capture the magnitude, and spatial and temporal variability in vegetation productivity for the region would be dramatically enhanced if future reanalyses can improve the representation of daily surface meteorology at northern latitudes.

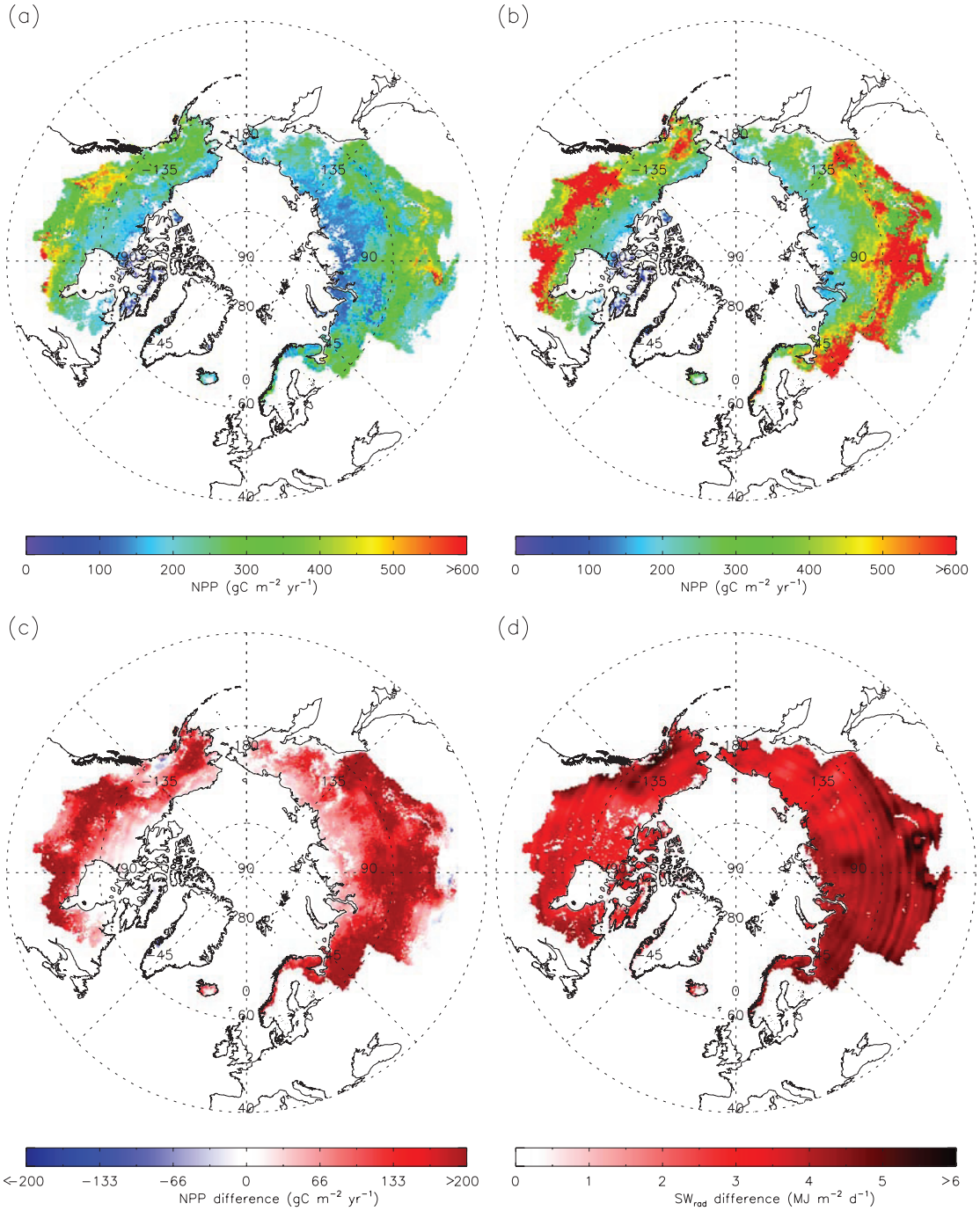

Figure 4. Mean annual NPP (g C m^{-2} yr^{-1}) derived from PEM calculations driven by (a) ERA-40 and (b) NNR over the pan-Arctic domain and 19-year (1982–2000) study period. The (c) NPP and (d) SW_{rad} difference maps refer to NNR less ERA-40 results.

3.3. PEM Derived Annual NPP Trends

[22] The spatial distribution of PEM based mean annual NPP (g C m^{-2} yr^{-1}) derived from the two reanalyses for the 19-year (1982–2000) study period are shown in Figure 4. The respective mean annual NPP calculations over the entire vegetated area were 257.5 ± 103.9[s] g C m^2 yr^{-1} and 398.3 ± 172.0 [s] g C m^2 yr^{-1} using ERA-40 and NNR inputs. Calculated mean annual NPP values for the major regional biomes are shown in Table 4. The NNR derived mean annual NPP was approximately 54.7% larger than the ERA-40 derived results. The primary reason for this discrepancy is that SW_{rad} from NNR was approximately 39.8% greater than ERA-40 radiation inputs for the region, while NNR T_{avg} inputs were approximately 1.1°C lower, on average, than ERA-40 temperatures. Higher SW_{rad} resulted in increases in PEM based GPP, while lower T_{avg} reduced calculated respiration rates; both of these factors resulted in relatively large increases in annual NPP calculations. A map of the mean SW_{rad} difference between the two reanalyses indicates that NNR solar radiation inputs exceeded the

Table 4. Comparison of PEM-Based NPP Results Derived From ERA-40 and NNR Inputs for the Major Biomes Within the Study Domain

	PEM NPP Driven by ERA-40, g C m^{-2} yr^{-1}		PEM NPP Driven by NNR, g C m^{-2} yr^{-1}		
Vegetation Type[a]	Uncorrected[b]	Corrected[c]	Uncorrected	Corrected	Observational Estimates, g C m^{-2} yr^{-1}
ENF	294.2 ± 99.4	167.0 ± 99.4	500.0 ± 149.9	178.8 ± 149.9	123 ∼ 460 for
DNF	248.8 ± 74.0	136.3 ± 74.0	438.1 ± 121.5	160.1 ± 121.5	Siberian and
Mixed forest	344.2 ± 113.1	201.6 ± 113.1	552.6 ± 158.3	191.1 ± 158.3	European forests [d] 225 for Alaska spruce [e] 226 ∼ 478 in central Canada [f]
Tundra	206.9 ± 75.1	123.0 ± 75.1	293.8 ± 114.8	120.4 ± 114.8	70 ∼ 500; mean: 90[g]
Grassland	248.6 ± 75.2	158.0 ± 75.2	312.9 ± 112.1	129.0 ± 112.1	137–477 [h]
Cropland	298.9 ± 99.0	181.3 ± 99.0	441.6 ± 152.8	144.6 ± 152.8	N/A

[a]ENF, evergreen needleleaf forest; DNF, deciduous needleleaf forest.
[b]Mean annual NPP ± standard deviations for 1982–2000 period.
[c]The average NPP difference from the sensitivity experiment was used as the error-correcting term.
[d]Values for Siberian and European forests [*Schulze et al.*, 1999].
[e]Values for mature spruce forests in central Alaska [*Ruess et al.*, 1996].
[f]Values for boreal forests in central Canada [*Gower et al.*, 1997].
[g]From *Saugier et al.* [2001] and *Shaver and Jonasson* [2001].
[h]From *Olson et al.* [2001].

ERA-40 values over most of the domain (Figure 4). On the basis of our comparisons of reanalysis and observed climate data, the ERA-40 surface meteorology appears to be relatively more reliable. Therefore the generally lower NPP results derived from the ERA-40 reanalysis may be more realistic than the more productive results derived from NNR.

[23] The Y parameter in equation (4) (i.e., the difference between mean annual NPP values derived from experimental data and original reanalysis data) provides an error-correcting term for adjusting NPP calculations to better reflect surface meteorological observations. The adjusted NPP results are summarized in Table 4 for the major regional biomes. These results are quite similar to NPP values reported in the literature for major vegetation types within the domain. Annual NPP for Arctic tundra has been reported to range from approximately 70 g C m^{-2} yr^{-1} for low tundra shrub communities of the high Arctic up to 500 g C m^{-2} yr^{-1} for tall shrub communities for the low Arctic, with an average level of approximately 90 g C m^{-2} yr^{-1} for the global tundra biome [*Saugier et al.*, 2001; *Shaver and Jonasson*, 2001]. Boreal NPP has been reported to range from 123 to 460 g C m^{-2} yr^{-1} for Siberian and European forests, respectively, on the basis of chronosequence studies and national forestry statistics [*Schulze et al.*, 1999]. NPP values for mature spruce forests in central Alaska were reported to be approximately 225 g C m^{-2} yr^{-1} [*Ruess et al.*, 1996], while values reported for boreal forests in central Canada range from 226 to 478 g C m^{-2} yr^{-1} [*Gower et al.*, 1997]. NPP observations for grasslands within the region range from 137 to 477 g C m^{-2} yr^{-1} and generally show intermediate levels of productivity between tundra and boreal forest biomes [*Olson et al.*, 2001].

[24] Despite large differences in SW_{rad} between ERA-40 and NNR, both data sets generally capture the 19-year meteorological trend for the domain (see section 3.1).

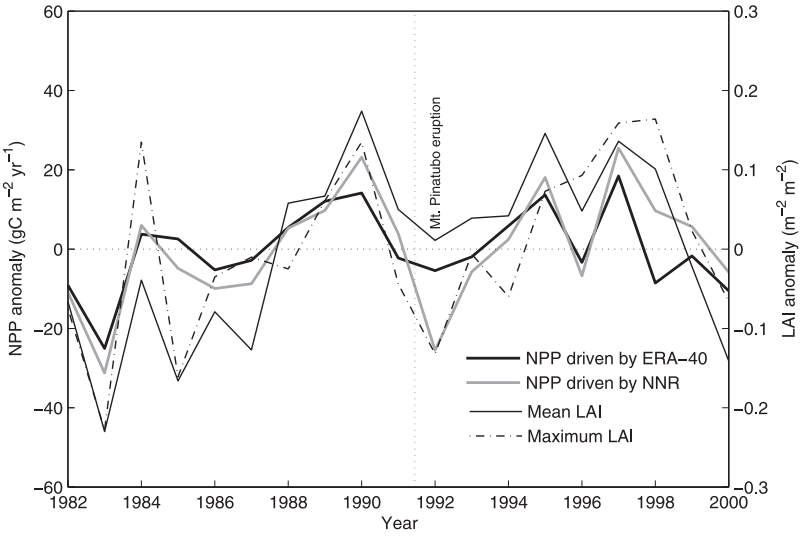

Figure 5. Calculated annual NPP anomalies for the pan-Arctic domain and 19-year study period using ERA-40 and NNR drivers for the PEM simulations; the AVHRR PAL derived mean and maximum annual LAI anomalies (relative to long-term mean) for the domain are also shown.

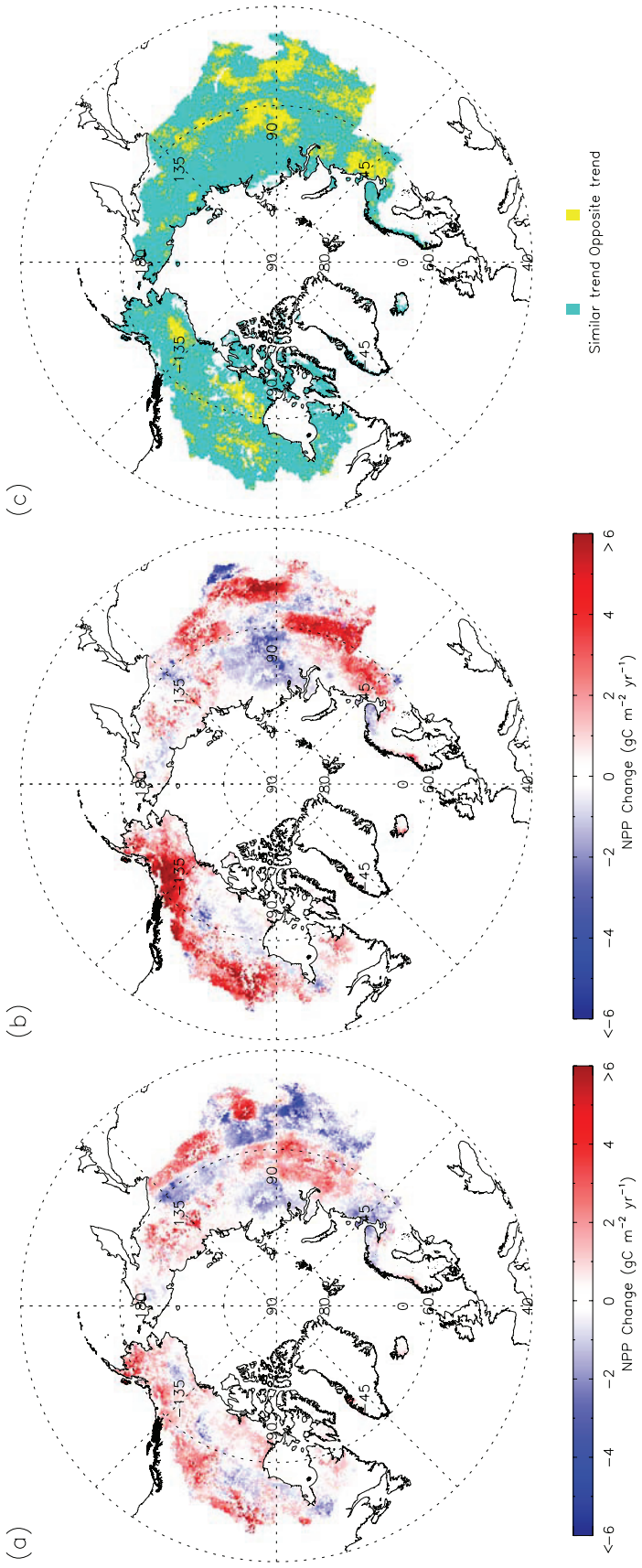

Figure 6. Spatial pattern of the multiyear trend in PEM based annual NPP (g C m^{-2} yr^{-1}) over the 19-year study period across the study domain excluding permanent ice and snow, open water and barren land as derived from (a) ERA-40 and (b) NNR inputs; (c) a map of associated differences in NPP trends from these results.

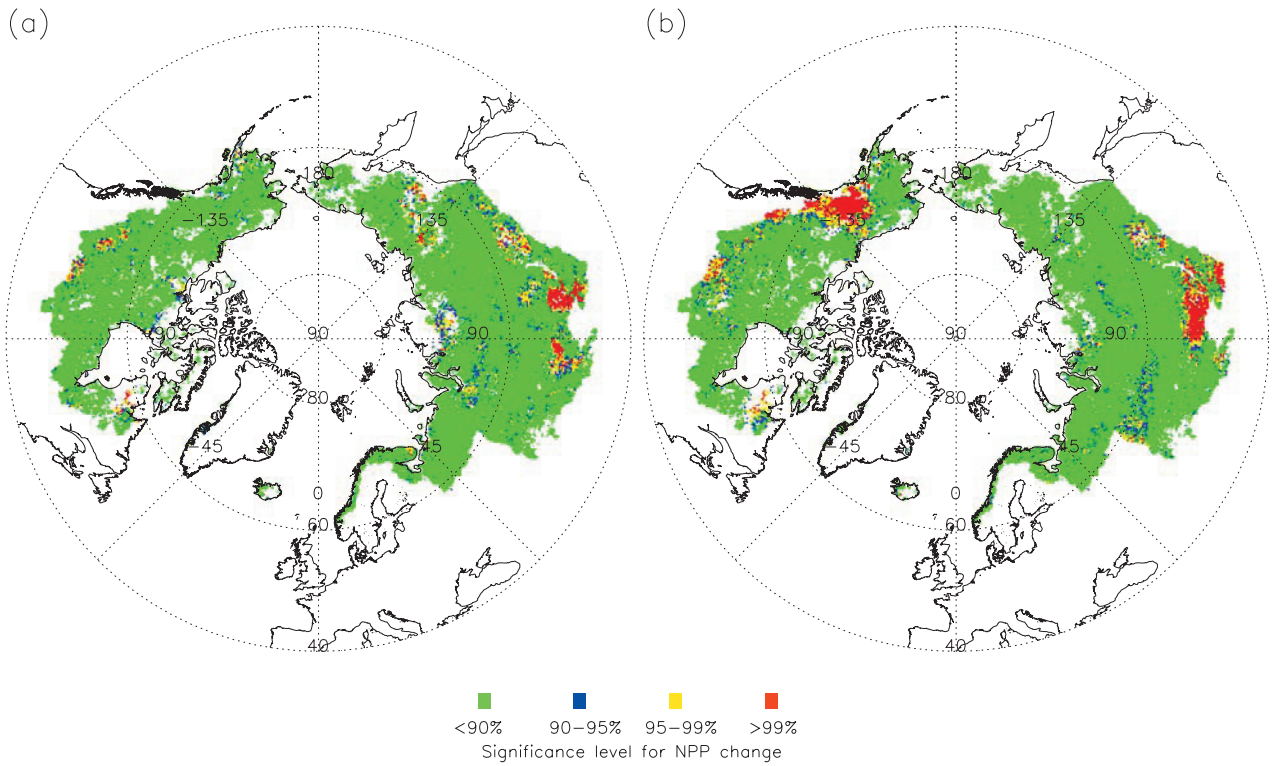

Figure 7. Spatial pattern of the statistical significance of the 19-year trends in annual NPP across the study domain excluding permanent ice and snow, open water and barren lands as derived from (a) ERA-40 and (b) NNR inputs.

Though our sensitivity analysis shows that the uncertainty in temperatures and SW_{rad} had the largest impact on PEM based NPP for both reanalyses, the comparison of annual variability in the model results indicates that this uncertainty does not result in large differences in NPP anomalies. The reason for this pattern is that SW_{rad} in both reanalyses shows only small and insignificant variability over the 19-year study period despite generally poor correspondence between reanalysis and observed SW_{rad} anomalies. In addition, reanalysis temperature anomalies were highly correlated with observed temperature anomalies. However, in some regions, for example, southern Alaska and southern Eurasia, reanalysis over predictions of SW_{rad} exaggerated predicted NPP magnitudes and temporal anomalies.

[25] Statistical analysis of these results indicated that annual NPP variability derived from both reanalyses was primarily driven by changes in terrestrial vegetation cover as detected by satellite LAI measurements ($r = 0.73$, $P < 0.001$ for PEM NPP driven by ERA-40; $r = 0.76$, $P < 0.001$ for PEM NPP driven by NNR). The positive trend in LAI and NPP for the 19-year period has been attributed to earlier thawing and increasing growing season length with regional warming [*Lucht et al.*, 2002; *Kimball et al.*, 2006]. Of the climatic variables, air temperature was the primary driver of annual NPP variability as derived from ERA-40 ($r = 0.22$, $P = 0.1840$) and NNR ($r = 0.45$, $P = 0.0264$) reanalysis climate drivers. The NPP response to air temperature was generally larger using NNR inputs relative to ERA-40, though calculated NPP anomalies and regional trends derived from both reanalyses were generally quite similar.

[26] The calculated annual NPP anomalies derived from the two reanalyses for the pan-Arctic domain and 19-year study period are shown in Figure 5. Calculated mean annual NPP for the entire vegetated domain increased by 0.372 g C m^{-2} yr^{-1} and 1.024 g C m^{-2} yr^{-1} over the 19-year period as derived from ERA-40 and NNR drivers, respectively. These regional trends are not statistically significant, though the temporal NPP trends for some regions were significant. Maps of the spatial pattern and statistical significance of the multiyear NPP trends are presented in Figures 6 and 7, respectively. The NPP results derived from the ERA-40 reanalysis indicate that 6.5%, 5.9% and 2.4% of the vegetated study region showed significant positive NPP trends at 90%, 95%, and 99% minimum probability levels, respectively. The NNR results showed larger proportions of significant positive trends, with 6.4%, 6.8% and 4.9% of the vegetated study region showing significant trends at the three respective probability levels.

[27] The PEM results from the two reanalyses showed similar NPP trends for 74.7% of the vegetated study region. The latitudinal and longitudinal distributions of the multiyear NPP trends for the domain also showed generally similar patterns between ERA-40 and NNR results, though NNR results showed larger variations (Figure 8). In regions above 65° N, the multiyear NPP trends showed close patterns between ERA-40 and NNR results, while NNR results showed much larger NPP trends in regions between 46°N and 62°N. In regions between 160° W and 130°W and

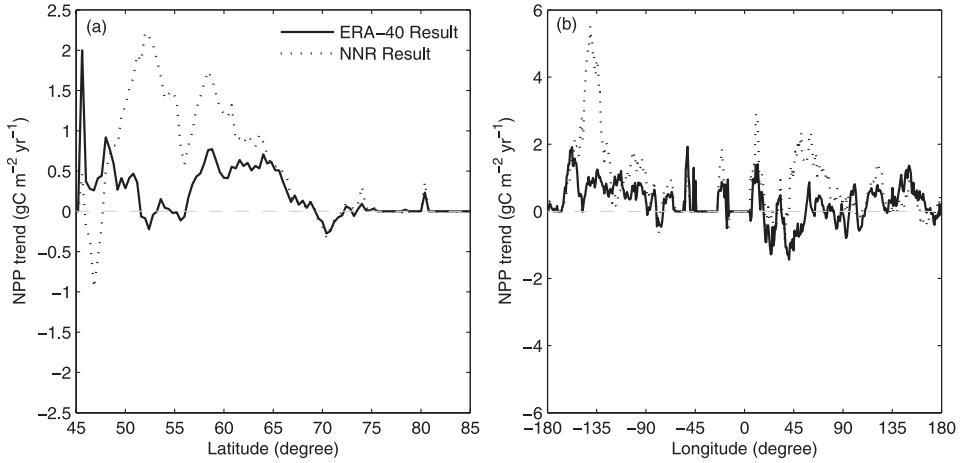

Figure 8. Mean (a) latitudinal and (b) longitudinal distributions of the 19-year trends in PEM based annual NPP (g C m^{-2} yr^{-1}) across the study domain as derived from the two reanalyses.

between 45°E and 90°E, NNR results also showed greatly exaggerated NPP trends relative to ERA-40 results. These latitudinal and longitudinal differences are largely due to over prediction of the NNR results across southern Alaska, and western and southern Eurasia relative to ERA-40 results (Figure 6). In this study, we only assessed the sensitivity and relative uncertainty of regional NPP simulations of the pan-Arctic basin and Alaska in response to uncertainties in surface meteorological inputs. However, model NPP results may also be negatively impacted by uncertainties in satellite remote sensing inputs including the PAL LAI/FPAR product, which incorporates uncertainties from dropped scan lines, navigation errors, data drop outs, edge-of-orbit composite discontinuities and other artifacts from the PAL NDVI [*Tucker et al.*, 2005]. A NASA Global Inventory Modeling and Mapping Studies (NASA GIMMS) NDVI product has attempted to correct most of the above problems and is currently available at 1/4 degree resolution [*Pinzon et al.*, 2004]. However, at the time of this investigation there was no alternative GIMMS LAI/FPAR product with similar spatial resolution to the 16 km PAL LAI/FPAR product.

4. Conclusions

[28] In this study, we identified major sources of uncertainty in ERA-40 and NNR based surface meteorology, and quantified associated impacts on regional NPP calculations for the pan-Arctic basin and Alaska. Considerable uncertainties in SW_{rad} and air temperatures (T_{min} and T_{avg}) resulted in over prediction of annual NPP by approximately 35.2 and 61.6 percent using ERA-40 and NNR inputs, respectively. Our results indicate that the ERA-40 daily surface meteorology is generally more accurate than the NNR, which is also consistent with previous studies [*Uppala et al.*, 2005; *Simmons et al.*, 2004; *Zhao et al.*, 2006]. While the magnitudes of the resulting fluxes are dramatically different, the two reanalysis products produced similar NPP spatial patterns for 74.7% of the domain, and similar annual anomalies and temporal trends. These results reflect partial reliance of the PEM on independent satellite remote sensing observations of LAI and FPAR, and the ability of the reanalyses to capture annual anomalies and regional trends in surface meteorology. A simple NPP correction method based on a sensitivity experiment between reanalysis and surface station meteorological measurements also produced generally consistent estimates of multiyear mean NPP for the six major biomes represented in the domain. These results confirm earlier observations and model based studies of a small, but predominantly positive trend in vegetation productivity for the northern terrestrial high latitudes during the 1980s and 1990s.

[29] Together these findings suggest that the ability of satellite remote sensing based productivity models to capture the magnitude and spatial and temporal variability in northern vegetation productivity would be enhanced if future reanalyses can improve the representation of daily surface solar radiation and air temperature. In particular, new regional reanalysis products able to resolve spatial heterogeneity approaching the resolution (approximately 25 km or less) of current global satellite remote sensing would enhance our ability to resolve cloud cover, terrain, and land use effects on surface meteorology and associated impacts to vegetation productivity. The NPP correction method may be useful for retrospective analyses, but may ultimately prove less beneficial for future studies than improvements in model reanalyses owing to a generally sparse and declining surface observation network at high latitudes. In addition to reanalysis inputs, considerable uncertainty is also introduced by satellite remote sensing based LAI/FPAR inputs from the monthly AVHRR PAL time series. These uncertainties are largely due to coarse spatial and temporal compositing of the remote sensing data used to mitigate frequent cloud cover and atmospheric aerosol effects. Further research is needed to address these limitations and improve confidence in regional NPP simulations for the northern high latitudes.

[30] **Acknowledgments.** The work was supported by grants from the National Science Foundation Office of Polar Programs and National Aeronautics and Space Administration's Earth Science Enterprise. Daily surface observations from WMO stations were provided by the National Climate Data Center. We thank NCEP/NCAR, ECMWF, NCDC, and

NSRDB for providing data sets. We also thank two anonymous reviewers for their insightful comments on an early draft of this paper.

References

Armstrong, R. L., and M. J. Brodzik (1995), An Earth-gridded SSM/I data set for cryospheric studies and global change monitoring, *Adv. Space Sci. Technol.*, *16*(10), 155–163.

Barber, V., G. P. Juday, and B. P. Finney (2000), Reduced growth of Alaskan white spruce in the twentieth century from temperature-induced drought stress, *Nature*, *405*, 668–673.

Bromwich, D. H., and R. L. Fogt (2004), Strong trends in the skill of the ERA-40 and NCEP-NCAR Reanalyses in the high and midlatitudes of the Southern Hemisphere, 1958–2001, *J. Clim.*, *17*, 4603–4619.

Bromwich, D. H., and S.-H. Wang (2005), Evaluation of the NCEP-NCAR and ECMWF 15- and 40-yr reanalyses using rawinsonde data from two independent arctic field experiments: Advances in high latitude numerical weather prediction, *Mon. Weather Rev.*, *133*(12), 3562–3578.

Bunn, A. G., S. J. Goetz, and G. J. Fiske (2005), Observed and predicted responses of plant growth to climate across Canada, *Geophys. Res. Lett.*, *32*, L16710, doi:10.1029/2005GL023646.

Churkina, G., and S. W. Running (1998), Contrasting climatic controls on the estimated productivity of different biomes, *Ecosystems*, *1*, 206–215.

Cihlar, J., et al. (1997), Multitemporal multichannel AVHRR data sets for land biosphere studies—Artifacts and corrections, *Remote Sens. Environ.*, *60*, 35–57.

Comiso, J. (2003), Warming trends in the Arctic from clear sky satellite observations, *J. Clim.*, *16*, 3498–3510.

DeFries, R. S., M. Hansen, J. R. G. Townshend, and R. Sohlberg (1998), Global land cover classifications at 8 km spatial resolution: the use of training data derived from Landsat imagery in decision tree classifiers, *Int. J. Remote Sens.*, *19*(16), 3141–3168.

Goetz, S. J., A. G. Bunn, G. J. Fiske, and R. A. Houghton (2005), Satellite-observed photosynthetic trends across boreal North America associated with climate and fire disturbance, *Proc. Natl. Acad. Sci. U.S.A.*, *102*(38), 13,521–13,525.

Gower, S. T., et al. (1997), Carbon distribution and above ground net primary production in aspen, jack pine and black spruce stands in Saskatchewan and Manitoba, Canada, *J. Geophys. Res.*, *102*(D24), 29,029–29,041.

Heinsch, F. A., et al. (2003), User's Guide: GPP and NPP (MOD17A2/A3) products NASA MODIS land algorithm, open file report, Univ. of Mont., Missoula.

Heinsch, F. A., et al. (2006), Evaluation of remote sensing based terrestrial productivity from MODIS using regional tower eddy flux network observations, *IEEE Trans. Geosci. Remote Sens.*, *44*, 1908–1923.

Helton, J. C., and F. J. Davis (2003), Latin hypercube sampling and the propagation of uncertainty in analyses of complex systems, *Reliab. Eng. Syst. Safety*, *81*, 23–69.

Helton, J. C., J. D. Johnson, C. J. Sallaberry, and C. B. Storlie (2006), Survey of sampling-based methods for uncertainty and sensitivity analysis, *Reliab. Eng. Syst. Safety*, *91*, 1175–1209.

Intergovernmental Panel on Climate Change (2001), *Climate Change 2001: The Scientific Basis—Contribution of Working Group I to the Third Assessment Report of the IPCC*, edited by J. T. Houghton et al., Cambridge Univ. Press, New York.

Kalnay, E., et al. (1996), The NMC/NCAR 40-year reanalysis project, *Bull. Am. Meteorol. Soc.*, *77*, 437–471.

Kimball, J. S., M. Zhao, K. C. McDonald, and S. W. Running (2006), Satellite remote sensing of terrestrial net primary production for the pan-Arctic basin and Alaska, *Mitig. Adapt. Strat. Global Change*, *11*, doi:10.1007/s11027-005-9014-5.

Kistler, R., et al. (2001), The NCEP/NCAR 50-year reanalysis: Monthly means CD-ROM and documentation, *Bull. Am. Meteorol. Soc.*, *82*, 247–268.

Lal, R., and J. M. Kimble (2000), Soil C pool and dynamics in cold ecoregions, in *Advances in Soil Science: Global Climate Change and Cold Regions Ecosystems*, edited by R. Lal, J. M. Kimble, and B. A. Steward, pp. 3–28, CRC Press, Boca Raton, Fla.

Lucht, W., et al. (2002), Climatic control of the high-latitude vegetation greening trend and Pinatubo effect, *Science*, *296*, 1687–1689.

McDonald, K. C., J. S. Kimball, E. Njoku, R. Zimmermann, and M. Zhao (2004), Variability in springtime thaw in the terrestrial high latitudes: Monitoring a major control on the biospheric assimilation of atmospheric CO_2 with spaceborne microwave remote sensing, *Earth Interact.*, *8*(20), 1–23.

Monteith, J. L. (1972), Solar radiation and productivity in tropical ecosystem, *J. Appl. Ecol.*, *9*, 747–766.

Myneni, R. B., R. R. Nemani, and S. W. Running (1997), Estimation of global leaf area index and absorped par using radiative transfer models, *IEEE Trans. Geosci. Remote Sens.*, *35*, 1380–1393.

Nemani, R. R., C. D. Keeling, H. Hashimoto, W. M. Jolly, S. C. Piper, C. J. Tucker, R. B. Myneni, and S. W. Running (2003), Climate-driven increases in global terrestrial net primary production from 1982 to 1999, *Science*, *300*, 1560–1563.

Oechel, W. C., G. L. Vourlities, S. J. Hastings, and S. A. Bochkarev (1995), Change in arctic CO_2 flux over two decades: effects of climate change at Barrow, Alaska, *Ecol. Appl.*, *5*, 846–855.

Oechel, W. C., G. L. Vourlities, S. J. Hastings, R. M. Zulueta, L. D. Hinzman, and D. L. Kane (2000), Acclimation of ecosystem CO_2 exchange in the Alaskan Arctic in response to decadal climatic warming, *Nature*, *406*, 978–981.

Oelke, C., T. Zhang, and M. C. Serreze (2004), Modeling evidence for recent warming of the Arctic soil thermal regime, *Geophys. Res. Lett.*, *31*, L07208, doi:10.1029/2003GL019300.

Olson, R. J., K. R. Johnson, D. L. Zheng, and J. M. O. Scurlock (2001), Global and regional ecosystem modeling: Databases of model drivers and validation measurement, *Tech. Memo. TM-2001/196*, Oak Ridge Natl. Lab., Oak Ridge, Tenn.

Pinzon, J., M. E. Brown, and C. J. Tucker (2004), Satellite time series correction of orbital drift artifacts using empirical mode decomposition, in *Hilbert-Huang Transform: Introduction and Applications*, edited by N. E. Huang, pp. 173–176, NASA Goddard Space Flight Cent., Greenbelt, Md.

Ruess, R. W., L. Van Cleve, J. Yarie, and L. A. Viereck (1996), Comparative estimates of fine root production in successional taiga forests of interior Alaska, *Can. J. For. Res.*, *26*(8), 1326–1336.

Running, S. W., and E. R. Hunt (1993), Generalization of a forest ecosystem process model for other biomes, BIOME-BGC, and an application for global-scale models, in *Scaling Physiological Process: Leaf to Globe*, edited by J. R. Ehleringer and C. B. Field, pp. 141–158, Elsevier, New York.

Running, S. W., P. E. Thornton, R. Nemani, and J. M. Glassy (2000), Global terrestrial gross and net primary productivity from the Earth Observing System, in *Methods in Ecosystem Science*, edited by O. E. Sala et al., pp. 44–57, Springer, New York.

Running, S. W., R. R. Nemani, F. A. Heinsch, M. Zhao, M. Reeves, and H. Hashimoto (2004), A continuous satellite-derived measure of global terrestrial primary productivity, *Bioscience*, *54*(6), 547–560.

Santer, B. D., et al. (2004), Identification of anthropogenic climate change using a second-generation reanalysis, *J. Geophys. Res.*, *109*, D21104, doi:10.1029/2004JD005075.

Saugier, B., J. Roy, and H. A. Mooney (2001), Estimations of global terrestrial productivity: Converging toward a single number?, in *Terrestrial Global Productivity*, edited by J. Roy, B. Saugier and H. A. Mooney, pp. 543–557, Elsevier, New York.

Schulze, E. D., et al. (1999), Productivity of forests in the Eurosiberian boreal region and their potential to act as a carbon sink—A synthesis, *Global Change Biol.*, *5*(6), 703–722.

Serreze, M. C., et al. (2000), Observational evidence of recent change in the northern high latitude environment, *Clim. Change*, *46*, 159–207.

Shaver, G. R., and S. Jonasson (2001), Productivity of arctic ecosystems, in *Terrestrial Global Productivity*, edited by J. Roy, B. Saugier and H. A. Mooney, pp. 189–210, Elsevier, New York.

Simmons, A. J., et al. (2004), Comparison of trends and low-frequency variability in CRU, ERA-40, and NCEP/NCAR analyses of surface air temperature, *J. Geophys. Res.*, *109*, D24115, doi:10.1029/2004JD005306.

Stocks, B. J., et al. (2002), Large forest fires in Canada, 1959–1997, *J. Geophys. Res.*, *107*, 8149, doi:10.1029/2001JD000484. [printed *108*(D1), 2003].

Sturm, M., C. Racine, and K. Tape (2001), Increasing shrub abundance in the Arctic, *Nature*, *411*, 546–547.

Thornton, P. E., and S. W. Running (1999), An improved algorithm for estimating incident daily solar radiation from measurements of temperature, humidity, and precipitation, *Agric. For. Meteorol.*, *93*, 211–228.

Tucker, C. J., et al. (2005), An extended AVHRR 8-km NDVI dataset compatible with MODIS and SPOT vegetation NDVI data, *Int. J. Remote Sens.*, *26*(20), 4485–4498.

Turner, D. P., W. D. Ritts, W. B. Cohen, S. T. Gower, M. Zhao, S. W. Running, S. C. Wofsy, S. Urbanski, A. Dunn, and J. W. Munger (2003), Scaling gross primary production (GPP) over boreal and deciduous forest landscapes in support of MODIS GPP product validation, *Remote Sens. Environ.*, *88*, 256–270.

Turner, D. P., et al. (2005), Site-level evaluation of satellite-based global terrestrial gross primary production and net primary production monitoring, *Global Change Biol.*, *11*(4), 666–684.

Uppala, S. M., et al. (2005), The ERA-40 re-analysis, *Q. J. R. Meteorol. Soc.*, *131*, 2961–3012.

Wang, X., and J. R. Key (2003), Recent trends in Arctic surface, cloud, and radiation properties from space, *Science*, *299*, 1725–1728.

Wang, X. L., V. R. Swail, and F. W. Zwiers (2006), Climatology and changes of extratropical cyclone activity: comparison of ERA-40 with NCEP-NCAR reanalysis for 1958–2001, *J. Clim.*, *19*, 3145– 3166.

White, M. A., P. E. Thornton, S. W. Running, and R. R. Nemani (2000), Parameterization and sensitivity analysis of the BIOME-BG C terrestrial ecosystem model: Net primary production controls, *Earth Interact.*, *4*(3), 1–85.

Yang, S. K., Y. T. Hou, A. J. Miller, and K. A. Campana (1999), Evaluation of the Earth radiation budget in NCEP-NCAR reanalysis with ERBE, *J. Clim.*, *12*, 477–493.

Zhao, M., F. A. Heinsch, R. R. Nemani, and S. W. Running (2005), Improvements of the MODIS terrestrial gross and net primary production global data set, *Remote Sens. Environ.*, *95*, 164–176.

Zhao, M., S. W. Running, and R. R. Nemani (2006), Sensitivity of Moderate Resolution Imaging Spectroradiometer (MODIS) terrestrial primary production to the accuracy of meteorological reanalysis, *J. Geophys. Res.*, *111*, G01002, doi:10.1029/2004JG000004.

J. Cassano, Cooperative Institute for Research in Environmental Sciences and Department of Atmospheric and Oceanic Sciences, University of Colorado, Boulder, CO 80309-0216, USA.

J. S. Kimball, S. W. Running, K. Zhang, and M. Zhao, Numerical Terradynamic Simulation Group, Department of Ecosystem and Conservation Sciences, University of Montana, 32 Campus Drive, Room 1224, Missoula, MT 59812-1224, USA. (zhang@ntsg.umt.edu)

W. C. Oechel, Global Change Research Group, Biology Department, San Diego State University, 5500 Campanile Drive, San Diego, CA 92182, USA.